

Article

Thermal Analysis of a Raft Concrete Foundation: A Case Study of a Leaking Ethane Tank

Chirawat Wattanapanich ¹, Thanongsak Imjai ^{1,*}, Pakjira Aosai ¹, Chayanon Hansapinyo ²,
Fabio P. Figueiredo ³ and Reyes Garcia ⁴

¹ School of Engineering and Technology, Walailak University, Nakhonsithammarat 80161, Thailand; wchirawa@wu.ac.th (C.W.); pakjira.ao@mail.wu.ac.th (P.A.)

² Center of Excellence in Natural Disaster Management, Department of Civil Engineering, Chiang Mai University, Chiang Mai 50200, Thailand; chayanon@eng.cmu.ac.th

³ School of Engineering, University of Minho, 4800-058 Guimarães, Portugal; f.figueiredo@civil.uminho.pt

⁴ Civil Engineering Stream, School of Engineering, The University of Warwick, Coventry CV4 7AL, UK; reyes.garcia@warwick.ac.uk

* Correspondence: thanongsak.im@wu.ac.th; Tel.: +66-(0)-7567-2378

Abstract: This article presents a case study on the thermal assessment of a reinforced concrete (RC) foundation exposed to low temperatures. The foundation supports a 19,500 m³-capacity tank with low-temperature (−89 °C) ethane. Icing and bubbling were observed on the tank's surface soon after it started operations. Condensation was also observed at the bottom of the 0.8-m-depth RC slab, which raised concerns about the structural condition of the concrete. This study provides details of the field and analytical investigations conducted to assess the structural condition of the foundation. Heat transfer finite element (FE) analyses were performed to examine the concrete sections subjected to low temperatures. It was found that the ethane leakage produced a low temperature on the top side of the concrete foundation of +9.7 °C. Overall, the temperatures calculated by the FE analyses were in good agreement with actual field measurements, within a ±5% accuracy. The simplified heat transfer equation for porous media used in this study was sufficiently accurate to model the effects of the ethane leakage in the concrete foundation, provided that the ambient temperature at the site is taken into account in the analysis. The results also confirm that reinforcing bars can be neglected in the thermal analysis of massive concrete slabs. The results from the field measurements and FE analyses confirmed that the structural integrity of the RC foundation was never compromised. The approaches, methods and techniques discussed in this article are deemed suitable to solve the practical and scientific challenges involved in the thermal assessment and repairs of large special structures. Accordingly, they can serve as useful reference and guidance for engineers and practitioners working in the field of forensic engineering.

Keywords: reinforced concrete; raft foundation; temperature effects; finite element modelling



Citation: Wattanapanich, C.; Imjai, T.; Aosai, P.; Hansapinyo, C.; Figueiredo, F.P.; Garcia, R. Thermal Analysis of a Raft Concrete Foundation: A Case Study of a Leaking Ethane Tank. *Buildings* **2022**, *12*, 889. <https://doi.org/10.3390/buildings12070889>

Academic Editor: Elena Ferretti

Received: 14 May 2022

Accepted: 21 June 2022

Published: 23 June 2022

Publisher's Note: MDPI stays neutral with regard to jurisdictional claims in published maps and institutional affiliations.



Copyright: © 2022 by the authors. Licensee MDPI, Basel, Switzerland. This article is an open access article distributed under the terms and conditions of the Creative Commons Attribution (CC BY) license (<https://creativecommons.org/licenses/by/4.0/>).

1. Introduction

Storage tanks in industrial facilities often store liquids and/or gases at extreme low (or high) temperatures at very high pressures. Many of such tanks are made of materials susceptible to corrosion (and erosion) at the contact zone where the phase of materials changes from liquid to gas, and vice versa. As a result of these drastic changes, serious incidents (or 'accidents') have been reported in tanks in the past [1]. Most of the storage tanks at petrochemical plants in Thailand are built on thick reinforced concrete (RC) foundations. Traditionally, these cast-in-place foundations are supported on piles and are therefore commonly referred to as 'raft foundations' [2]. The raft foundations then support the storage tanks. Raft RC foundations have proven to be a cost-effective and reliable structural solution to support storage tanks in the petrochemical industry. However, the construction of such raft foundations requires strict quality control and quality assurance, as well as

periodic inspection and maintenance to guarantee the integrity of the foundations over the service life of the tanks [3–5]. This is important from a structural engineering point of view because the changes in temperature in the tank can in turn lead to changes in the mechanical properties of concrete, such as its compressive and tensile strengths [6,7].

Ethane storage tanks are very common in petrochemical plants. Liquid ethane has a very low boiling point and turns into gas at ambient temperature. However, liquid ethane can reach extremely low temperatures well below 0 °C. In the case of unexpected leakages, part of the concrete surface in the foundation can be subjected to extremely low temperatures (up to −20 °C), which in turn can also lead to damage [8–11]. Previous research has shown that the strength of both concrete and reinforcement tends to increase when the temperature reduces within a particular range (e.g., 20 °C to −40 °C) [11–15]. This effect is particularly evident in moist concrete, where the increase in compressive strength has been attributed to the formation of ice which increases progressively as the temperature reduces [16]. For steel reinforcement subjected to low temperature, experiments have shown that reinforced bars tend to become brittle when exposed to extremely low-temperature environments (less than −20 °C) [11–15]. Other studies have also investigated fatigue and thermal effects on concrete [17]. On the other hand, test results indicate that steel reinforcement subjected to extreme low temperature (below −20 °C) tends to become brittle. While unlikely, the potential leakage of ethane is possible even if quality control and quality assurance procedures were followed during construction of the foundation and the tank. However, to date there are limited guidelines [18,19] on how to assess the effect of unexpected leakage of extreme low-temperature liquids on the overall structural integrity of concrete foundations, especially for practical case studies. Moreover, only a few studies have investigated numerically the changes in temperature of structural elements under specific, realistic temperature profiles [20–22].

The structural inspection of raft foundations of storage tanks has significant challenges due to the peculiarities of these special structures. For instance, excavations around the foundation and in situ load testing are often required to identify damage. Concrete core sampling/testing can also provide some relevant information on the concrete properties. However, coring can be very challenging (due to the limited working space under the foundation slab) and time consuming and can sometimes produce damage to the foundations. Limitations always exist as potential defects between the foundation and the tank cannot be easily detected by simple visual inspections. To bypass some of these limitations, nondestructive tests (NDTs) can be used to assess the condition of concrete foundations for tanks. Whilst it has been claimed that NDTs can help assess the structural integrity of structures without the need for excessive concrete coring or load testing [23–25], it is always preferred to validate NDT test results with core test results, whenever possible.

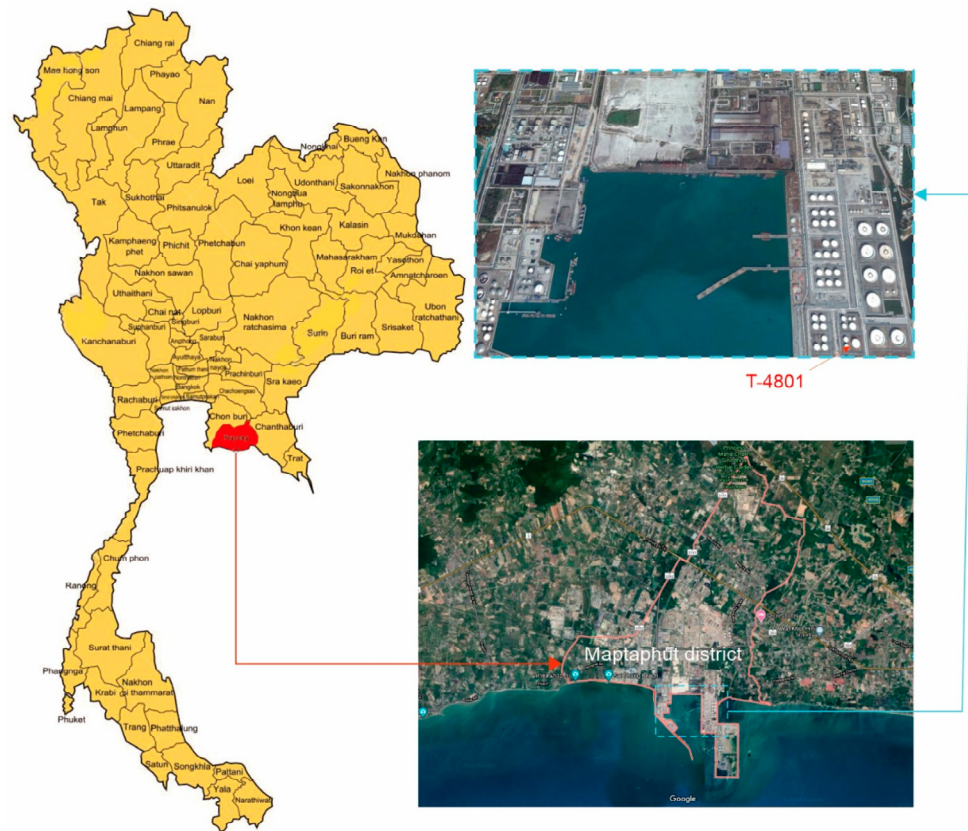
Another challenge arises when concrete is exposed to very low temperatures. Under this condition, the capillary water changes phase from liquid to solid, which increases the water's volume, and chemically bound water is released due to hydration. This results in an increase in pore pressure, which is believed to be one of the mechanisms leading to concrete spalling in structures exposed to extremely low temperatures of less than −20 °C [11,12]. Several mathematical models to simulate the thermal behaviour of concrete exist in the literature. Most of these models are based on the theory of heat and mass transfer in porous media and have been implemented in finite element (FE) software [14,26]. Vapour diffusion, liquid water flow due to pressure gradients, capillary effects, and evaporation/condensation are the main characteristics observed in porous media such as concrete [27–29]. Due to the complexity of the nonlinear phenomena involved in porous media at extremely high or low temperature, a fully coupled mathematical model is necessary to predict the evolution of temperature and pore pressure.

This article presents a case study on the thermal assessment of a circular RC foundation exposed to low temperatures. The foundation supports one of the largest storage tanks in Thailand, and it is part of a large petrochemical plant. Because most of the information in the subject is limited and/or scattered, this study aims to summarise the approaches, methods and techniques used to solve the practical and scientific challenges involved in the structural assessment and repairs of this large special structure that presented issues soon after it started operating. Indeed, the storage tank leaked ethane that spilled to the RC foundation, which raised structural safety concerns to the stakeholders. A numerical finite element (FE) model is developed to simulate the temperature changes of the RC foundation subjected to temperature profiles of the ethane leakage. Issues related to the computational strategy for heat transfer problems are then reported and commented upon. The FE results are compared with field temperatures measured at the bottom of the foundation. Finally, the results from the FE simulation are analysed and discussed. This article is an addition to the very few studies that have investigated numerically the changes in temperature of structural elements. The approaches, methods and techniques adopted in this study can serve as useful reference and guidance for engineers and practitioners working in the field of forensic engineering.

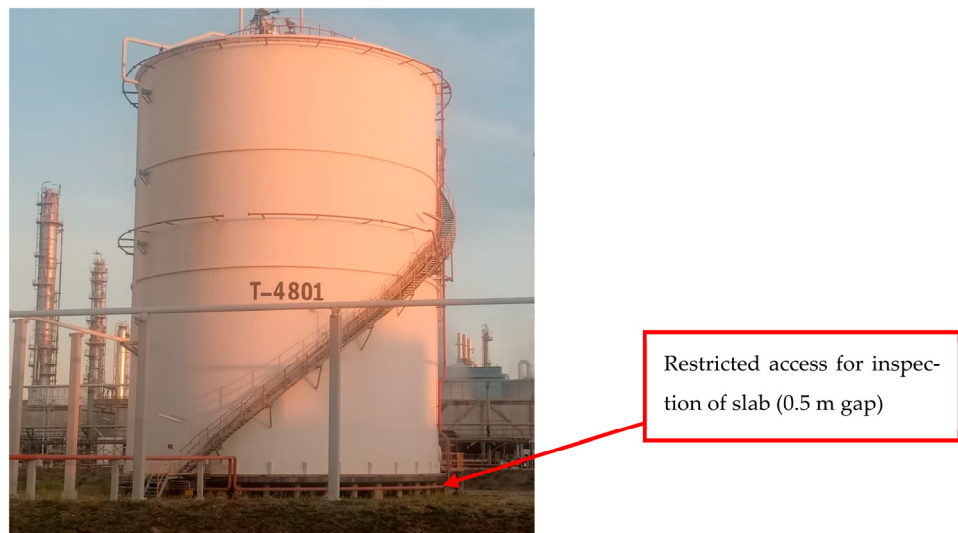
2. Case Study: Ethane Storage Tank

2.1. General Characteristics

The storage tank is part of a petrochemical plant at the Ta Phut Industrial Estate, Rayong Province, Thailand. Figure 1a shows the location of the plant. The construction of the plant was completed in late 2010 [30], after which it started operations. The plant includes the T-4801 ethane storage tank shown in Figure 1b. This is a single containment tank with an internal diameter of 28.5 m, a height of 30.6 m, and a total capacity of 19,500 m³. The 35 mm thick walls of the tank are made of stainless/carbon steel Grade 304 according to ASTM A240 [31]. The tank stores liquid ethane (C₂H₆) for gas processing and therefore operates at an extremely low temperature of −89 °C and at a pressure of 500 mH₂O. The tank is not insulated but only protected with a fireproof coating, according to local regulations. A raft RC slab of depth 0.8 m supports the tank. The slab sits on 122 square (0.4 × 0.4 m) concrete piles of 7.0 m height typically spaced at 2.0 m at the central zone of the slab, and at 1.5 m at its circumferential zone (see typical distance TYP. in Figure 2b). The bottom of the slab itself is at only 0.5 m above the ground level (Figures 1c and 2c). Such small gap provides just enough headroom to perform periodic inspections of the foundation. It should be noted that this gap was not part of the original construction project and that the slab was originally touching the ground. However, partial settlement gradually developed and a 0.5 m gap was observed at the time of inspection.



(a)



(b)

Figure 1. (a) Location of T-4801 ethane tank within the Ta Phut Industrial Estate, and (b) T-4801 ethane tank [30].

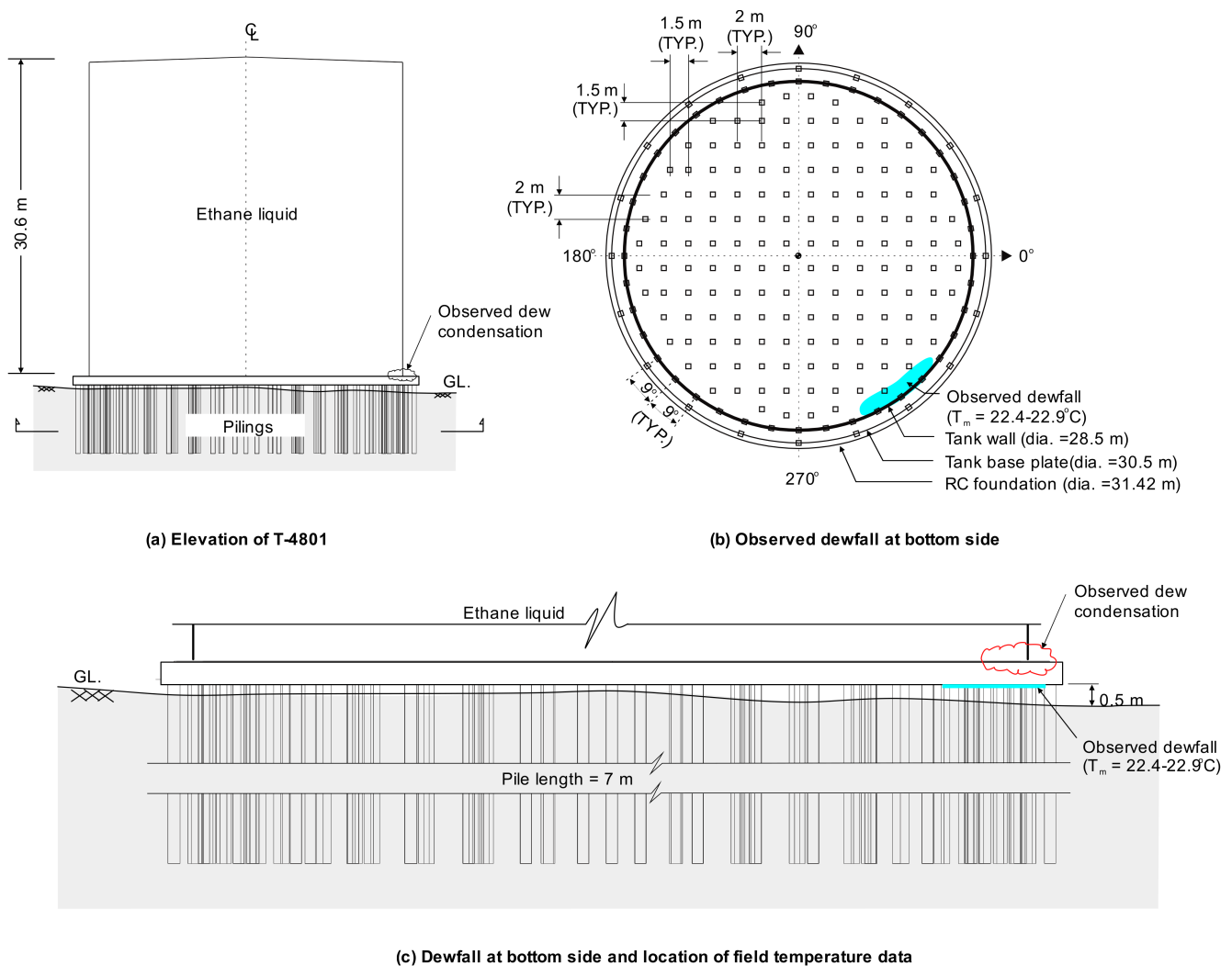


Figure 2. (a) Elevation of T-4801 tank, (b) plan view of foundation and location dew at the outer shell wall plate and bottom plate, and (c) lateral view of foundation and location of dew fall.

2.2. Inspections and Repairs

Icing and bubbling were reported to occur on the tank's wall and base plate in early 2011, at the location shown schematically in Figure 2a. A visual inspection performed at the bottom of the RC foundation revealed the presence of dew at the periphery around the annular space. In particular, dew condensation was observed at an orientation of about 310° , as shown in Figure 2b. The icing disappeared after three weeks, but the dew remained on the tank's wall and base plate. In addition, the dew condensation was also observed at some parts of the welded joints between the outer shell wall plate and bottom plate. Visual testing (VT) and ultrasonic testing (UT) methods were performed according to ASTM [32] to assess the integrity and defects of the welded joints of the tank. The test results confirmed a small defect in the welding. From the inspection results, it was concluded that a more detailed engineering assessment (DEA) and more thorough periodic inspections were necessary to discard further structural issues.

A preliminary inspection detected dew condensation at some parts of the welded joint between the outer shell wall plate and bottom plate of the steel tank, with the evidence of ethane leakage in an area of approximately $5 \times 2 \text{ m}^2$. Therefore, it was concluded that urgent repairs were needed at the welded joints to maintain the functionality of the tank. However, as the stakeholders decided to keep the tank fully operational during the repairs, the preliminary inspection was limited to the outer part of the tank. Accordingly, it was not

possible to determine other potential damage inside the tank. The repairs were completed in March 2011. No cracks and/or spall of concrete were observed at the bottom side of the RC foundation, and this was confirmed by UPV tests.

A follow-up inspection was carried out after three months of the repairs on the welded joints. Despite the repairs, dew was still observed at the tank's bottom, at the same location where the leak was initially observed. As a result, it was decided to empty the tank to inspect the leakage in more detail. The dew was present at the bottom of the RC foundation (Figure 2c) as the liquid ethane leaked from the welded joint inside the container and remained at the bottom of the tank, thus producing the dew observed at the bottom of the foundation (due to thermal conduction through the concrete). After emptying the tank, access was possible to the outer shell wall and bottom plates from the inside of the tank, which allowed the repair of the affected area (about $5 \times 2 \text{ m}^2$, as shown in Figure 2b) that caused the ethane leaks. The good quality of the welding repairs was verified using UPV techniques [18].

The work on the tank was divided into two phases. Figure 3 shows the flowchart of the inspections performed in Phase 1. In Phase 1 and following the preliminary inspections (items 1 and 2 in Figure 3), a DEA was carried out to assess more thoroughly the structural condition of the foundation and to obtain the thermal properties of the concrete via NDTs (item 6 and 7 in Figure 3). The results from Phase 1 were subsequently used in Phase 2 to perform thermal integrity analyses to dilT scard potential damage in the RC foundation as a consequence of the leakage. Detailed results from the NDTs in Phase 1 were presented by the authors previously [33,34]. Further details on Phase 1 and all Phase 2 are described in the following sections.

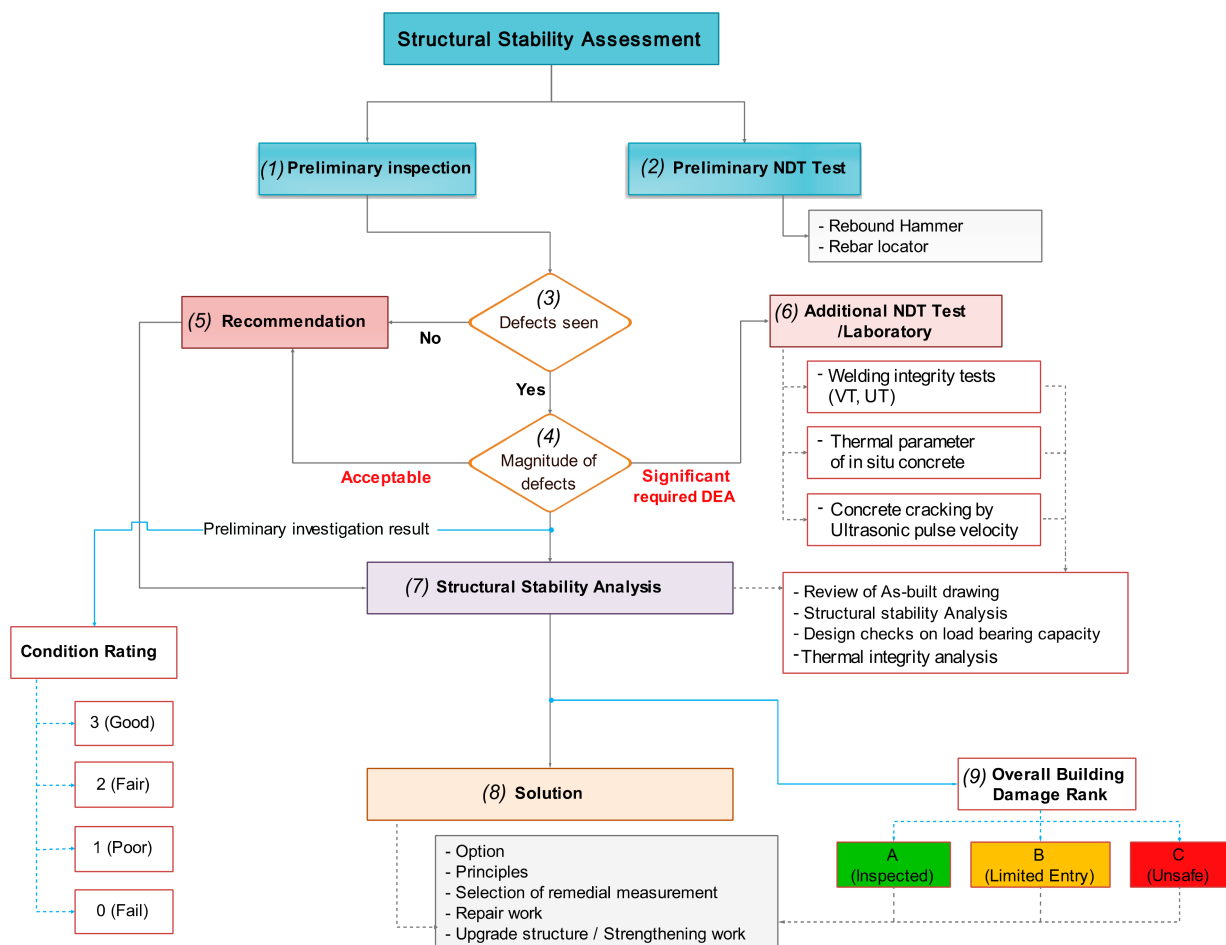


Figure 3. Flowchart of work in Phase 1 (adapted from Imjai and Tungsanga [33]).

3. Phase 1: Inspection of the T-4801 Tank

The main aims in Phase 1 were to identify structural deterioration and to determine the preliminary serviceability condition of all the structural components of the tank. The inspection was performed according to the ACI 364 [35] standard, whereas the damage rating condition complied with the RILEM TC 104 guidelines [18]. The steel tank structure was also inspected in accordance with the manual and guidelines of the American Petroleum Institute (API) [18]. Special attention was paid to assessing the condition of the welded joints of the steel tank, which was performed according to the API specifications [18,36]. The visual inspection was limited to accessible areas of the tank, as well as to the accessible parts of the bottom of the RC foundation (see Figure 1b). Accordingly, there may have been inaccessible areas or parts of the tank/foundation with some damage that was not visible because they were covered and/or blocked by staircases, fire hoses, etc. To examine the structural integrity of the tank, design checks on load-bearing capacity with the actual material properties at the time of construction were also performed.

3.1. Field Temperature Measurements

Two datasets of temperature (shown in Appendix A) were obtained using thermal sensors. Dataset 1 was obtained by the staff of the petrochemical plant, who measured the temperatures at the bottom side of the concrete foundation soon after the ethane leakage was observed. The authors obtained Dataset 2 one week after the repairs of the welded joints were completed. To achieve this, a thermal resistance temperature detector (RTD) sensor (Figure 4) with a measurement range of $-100\text{ }^{\circ}\text{C}$ to $+330\text{ }^{\circ}\text{C}$ was used to measure the temperature at the bottom of the RC foundation. The thermal sensor was calibrated by the manufacturer before use. Moreover, just before the field measurements, the thermal sensor readings were compared with laser temperature readings in hot and cold water. The temperature readings in both cases were the same. The measurements were limited to accessible locations where condensation was observed. Temperature data were collected at three different locations (0, 50 and 100 mm) measured from the bottom of the concrete slab. To fix the sensor to the concrete, a 4 mm hole was first drilled. Then the dust inside the hole was removed using an air blower, after which the hole was filled in with a thermal grease of extremely high thermal conductivity. The field temperature was monitored for 24 h and transmitted to a data acquisition system in real time. The relative humidity and wind speed were also recorded on the day of the field inspection.



Figure 4. High precision thermal RTD sensor (RTD-1PT100K2515-36-T) and data acquisition system.

3.2. Material Properties and Design Checks on Load Bearing Capacity

The physical and thermal properties of the concrete exposed to low temperatures were obtained to provide data for FE modeling. Only twelve cores were extracted as coring was very challenging due to the limited working space under the foundation slab (0.5 m only). The testing points were selected based on the original construction drawings followed by a walk-through around the foundation. The concrete compressive strength was obtained from NDT rebound hammer tests and from compression tests on six core samples (diameter = 100 mm). The average concrete compressive strength was 24.0 MPa, the dry density was 2355 kg/m^3 , and the calculated elastic modulus was 23,025 MPa based on the ACI-318 equation [37]. Comparatively, the original (cylinder) design compressive strength was 21.0 MPa. These initial results suggested that the concrete under the slab was unlikely

to be exposed to very low temperatures. Additionally, the other six concrete cores were sliced into 10-mm-thick samples to examine the thermal properties of the concrete according to ASTM C177-19 [38]. The average conductivity and specific heat of the concrete were found to be 2.56 W/m °C and 0.88 kJ/kg °C, respectively. The results from these samples were later fed into the numerical analysis. The original drawings of the RC foundation specified a yield strength of the reinforcing bars equal to 392 MPa for the flexural (Ø25 mm) and shear (Ø16 mm) bars. The concrete cover (75 mm) and location/size of reinforcing bars were verified using ferro scanning techniques.

The structural assessment and DEA of the ethane tank structure was performed according to Eurocode 3 and AISC specifications [39], as well as ACI 318 [37]. The ultimate capacity of the RC members and applied factored loads were considered. The calculations confirmed that, as expected from a relatively new structure, the capacity of the existing steel tank and concrete foundation were adequate to resist the original design loads.

4. Phase 2: Thermal Integrity Analysis

An inverse numerical analysis was carried out to investigate the effect of the low temperature on the concrete slab. It should be noted that whilst an inverse numerical analysis was adopted in this study, such analysis may not be the best approach to do thermal analysis of other structures. This study employed an inverse analysis to assess the slab mainly because it was impossible to measure the temperature at the top face of the slab (i.e., just under the ethane tank at the tank-foundation interface), and therefore, only temperature data measured at the bottom of the slab (Section 3.1) was available for comparisons.

4.1. Heat Transfer in Concrete Slab

In this study, the concrete of the foundation was modeled as a porous media material where the voids of the solid skeleton were filled with liquid and gas. The heat transfer in the foundation was examined using the computational fluid dynamics (CFD) module of the FE software COMSOL Multiphysics [40]. This software was chosen because (i) it has a stable solver for both linear and nonlinear problems, and (ii) it has an extensive library of elements which can be used to model concrete subjected to thermal loading. In COMSOL, one of the most important steps was choosing the appropriate physics for the model, adding physics conditions and constraints, and assigning the physics to foundation geometric entities. In this study, the “Heat Transfer” physics was used by choosing the heat transfer in porous media library added into the model. The time-dependent heat transfer in the solid interface was numerically computed by solving the heat equation and the momentum balance equation [40,41], as shown in Equation (1).

$$\rho C_p \left(\frac{\partial T}{\partial t} + u_{trans} \cdot \nabla T \right) + \nabla \cdot (q + q_r) = -\alpha T : \frac{dS}{dt} + q \quad (1)$$

where ρ is the density of the material (SI units: kg/m³), C_p is the specific heat capacity at constant stress (J/kg·K), T is the absolute temperature (K), u_{trans} is the velocity vector of translational motion (m/s), q is the heat flux by conduction (W/m²), q_r is the heat flux by radiation (W/m²), α is the coefficient of thermal expansion (1/K), S is the second Piola-Kirchhoff stress tensor (Pa), and q contains the additional heat sources (W/m³).

For a steady-state problem, the temperature does not change with time, and the terms with time derivatives disappear. The heat transfer equation for porous media can be derived from the mixture rule on energies appearing in solid and fluid heat transfer equations [42]. Accordingly, Equation (1) can be simplified to

$$\rho_s C_{p,s} \frac{\partial T_s}{\partial t} + \nabla \cdot q_s = Q_s \quad (2)$$

where ρ_s is the solid and fluid densities (kg/m^3), $C_{p,s}$ is the solid heat capacity at constant pressure ($\text{J}/\text{kg}\cdot\text{K}$), q_s is the solid conductive heat flux (W/m^2), and Q_s is the solid heat source (W/m^3).

Previous studies have shown that the heat transfer through porous materials such as concrete was successfully simulated using Equations (1) and (2) and COMSOL Multiphysics [26,43,44].

4.2. FE Modelling, Boundary Conditions and Thermal Effects

Figure 5a shows the plan view and cross section of the model of the concrete foundation. 3D-solid hexahedron elements with eight-noded elements (global mesh size = 200 mm) with three degrees of freedom at each node (three translations in x, y and z directions) were used to model both the slab (diameter = 31.4 m; overall thickness = 0.8 m) and the concrete piles (square section = 0.4×0.4 m). This element type is less sensitive to distortion, and hence it was preferred over brick element to better model the circular geometry of the slab. The hexahedron elements (see Figure 5b for close up view of mesh for quarter of slab) also have higher coarse mesh accuracy over 3D tetra or wedge elements. This element is based on the displacement mode separation method. The element passes the constant stress patch tests, shows a low mesh distortion sensitivity and high accuracy in shell applications. Moreover, the element maintains an adequate element size along the whole section of the foundation to minimise potential issues with numerical instabilities. It should be mentioned that COMSOL optimises the mesh size, which in this case led to a total cell number of 77,535 elements. At the time of the field inspection, the tank was empty due to the repair works in the welded joints, and therefore, the steel tank and gas loading were not included in the analysis. The default penalty method for contact characteristics (used to simulate the contact between the deformable and rigid objects defined by COMSOL) were used to simulate the contact between slab and piles. Because the mass and volume of the concrete slab are massive compared to those of the reinforcing bars (volume of bars was only 3.75% of total), the bars were not included in the modeling as these were expected to have a negligible effect in the results, as reported in previous studies [43,44]. Figure 5c illustrates a quarter of slab showing the thermal boundary conditions.

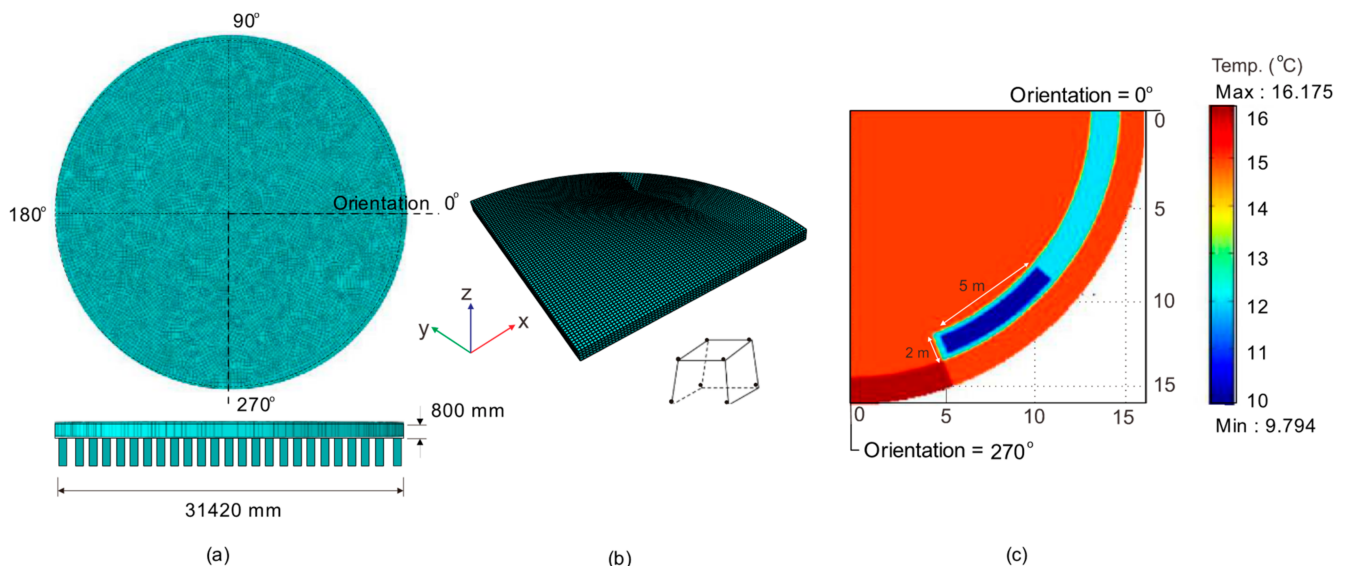


Figure 5. (a) Plan view and cross section of 3D FE mesh of the slab; (b) Close-up view of mesh for quarter of slab, and (c) quarter of slab showing the thermal boundary conditions.

A default penalty method available in COMSOL contact library was adopted and used in the analysis. The penalty method offers a more stability from the convergence, is more robust, and requires less computational time. In this case, a sliding between concrete pile and foundation can be considered as small, but no separation was left between the contacting pairs. Table 1 summarises the linear elastic material properties and thermal characteristics of the concrete used in the analyses.

Table 1. Concrete parameters used in the FE analyses.

| Parameter | Value | Unit |
|--|---------------------|-------------------|
| Concrete density, ρ | 2300 | kg/m ³ |
| Thermal conductivity, k | 2.56 | W/m·C |
| Specific heat capacity, C_p | 0.88 | J/Kg·C |
| Coefficient of thermal expansion, α | 10×10^{-6} | 1/C |
| Young modulus, E_c | 23,025 | MPa |
| Poisson's ratio, ν | 0.31 | - |

The boundary temperature assumed in Step 1 of the numerical analysis (Figure 5b) was applied to the top side of the slab on an area of $5 \times 2 \text{ m}^2$ (see Figure 2b), which was the approximate area of ethane leakage under the tank. To reduce computational time, only a quarter of the concrete foundation was modeled, as shown in Figure 5b.

To determine the top temperature distribution of the foundation (which had unknown boundary conditions), an iterative inverse numerical FE analysis was implemented. In Step 1, a temperature distribution was assumed at the top of the slab (at the location of interest). Next, heat transfer numerical analyses were implemented (in Step 2) by solving the heat transfer equations for porous media. Subsequently, the temperature distribution at the bottom of the slab calculated by the FE models was compared to the field temperature data (Step 3). The FE analyses were repeated by changing the assumed temperature distribution (in Step 1) until the analytical results matched the measured temperatures (Datasets 1 and 2) within a 5% accuracy.

5. Results and Discussion

5.1. Temperature Distribution along the Concrete Foundation

Figure 6a shows the temperature distributions at the top of the slab calculated by the FE simulations. The results indicate that maximum temperatures of $+9.7 \text{ }^\circ\text{C}$ were distributed over the possible leakage location. Figure 6b,c shows the temperature profile at different cross sections along the 0° and 270° orientations of the foundation. The results show that the temperature at the bottom of the foundation was $+17.8 \text{ }^\circ\text{C}$ when the temperature at the top of the slab was $+9.7 \text{ }^\circ\text{C}$.

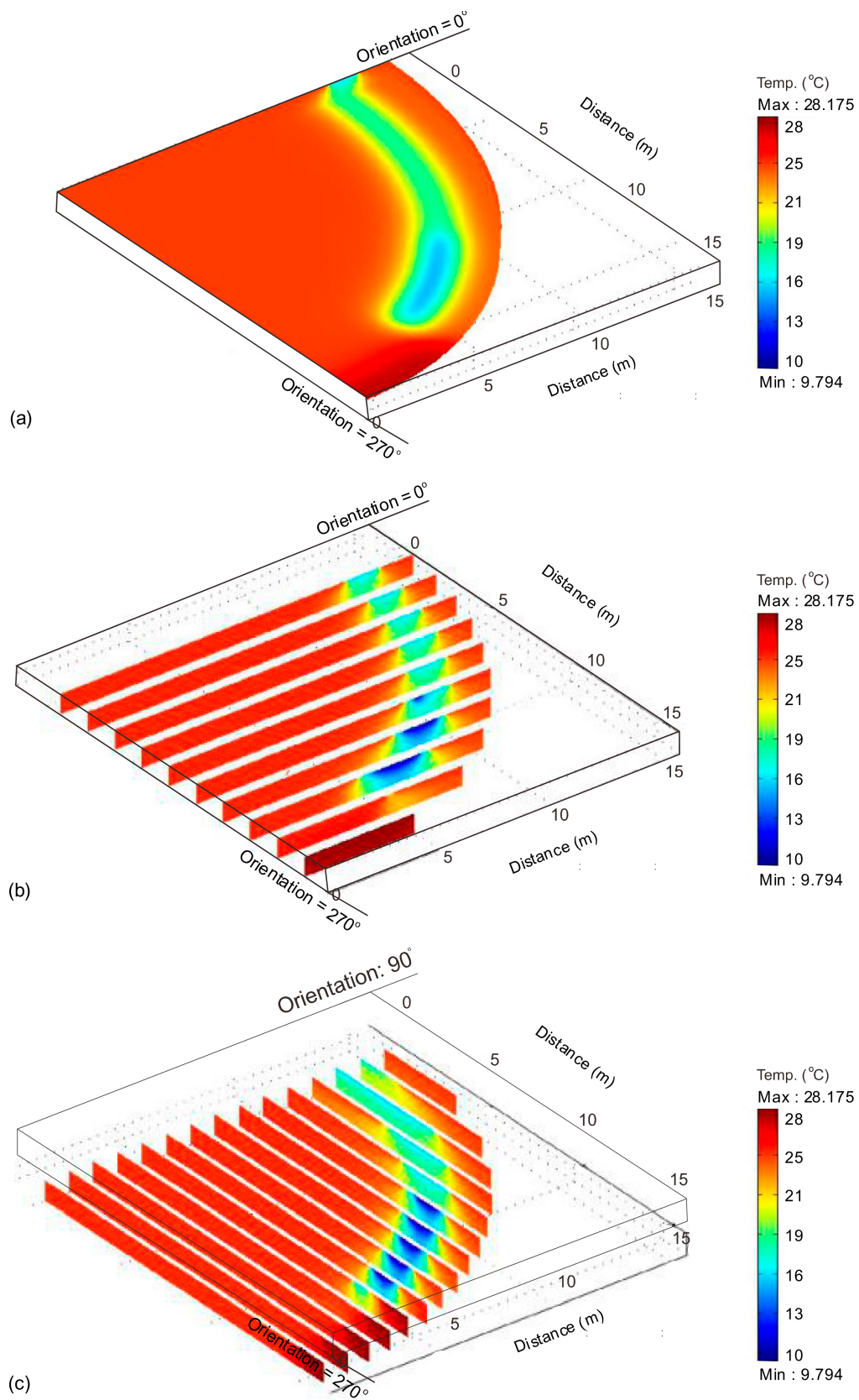


Figure 6. Temperature profile across concrete foundation; (a) temperatures at the top of the slab, (b) along orientation 0°, and (c) along orientation 270° orientation.

5.2. Effect of Ambient Temperature

Figure 7 shows the effect of the ambient temperature on the temperature profile across the slab. The ambient temperature at the site was recorded from 14:00 h onwards, and it was found to vary between +18.4 and +23.9 °C during the field temperature measurements in Phase 1. The average relative humidity (RH) measured at the site was 82%, with a sunny environment. Figure 7 also shows the temperature gradient over the cross sections of the slab at 130° orientation subjected to a temperature of +9.7 °C applied to the top of the foundation, which increases to +15.8 °C at the bottom of the slab without ambient temperature introduced in the model.

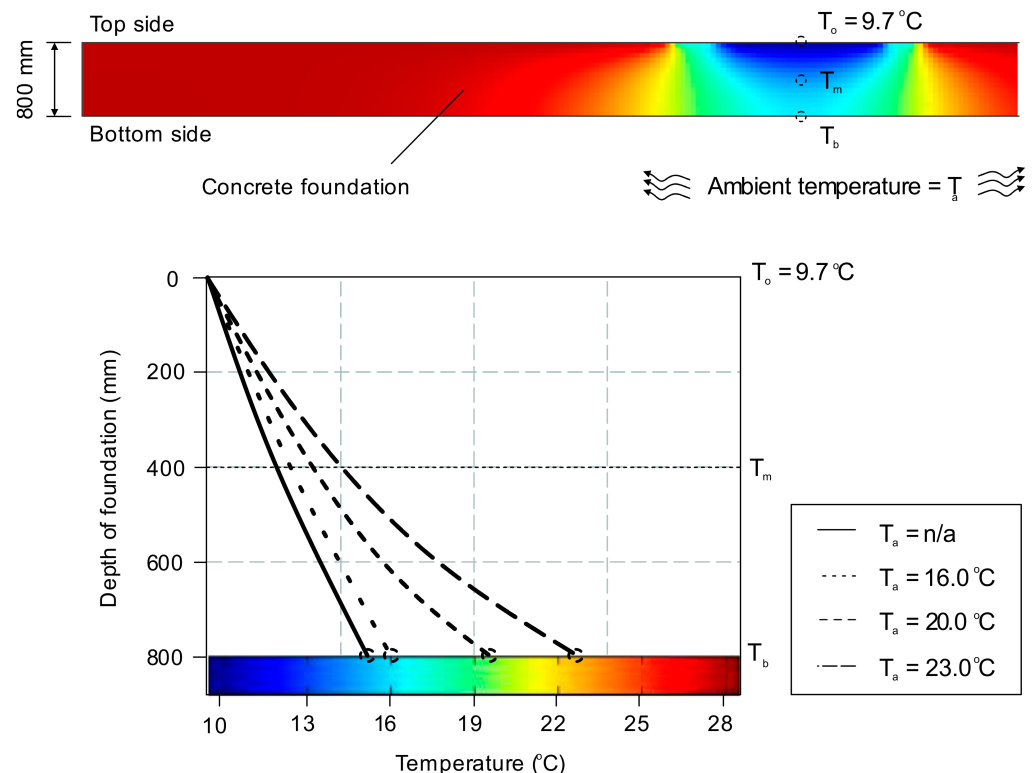


Figure 7. Temperature profile along the cross section of concrete foundation at 310° orientation with the effect of ambient temperature.

The effect of the ambient temperature (T_a) was taken into account by inputting different values of T_a into the FE model. Parametric studies on the effect of T_a (by setting $T_a = +16\text{ °C}$) showed that the predicted temperature at the bottom of the slab was 30% lower than the measurements, although such difference reduced to 13% by setting $T_a = +20\text{ °C}$. A value $T_a = +23\text{ °C}$ (i.e., the temperature recorded during the field inspection) led to a good match with the temperatures from the field measurements. Indeed, the ratio between the measured and calculated temperatures (Exp/FE) and standard deviation (SD) were 1.03 and 0.03 for Dataset 1, respectively. Such values were Exp/FE = 1.05 and SD = 0.04 for Dataset 2 (see Appendix A). Figure 7 also shows that the temperature progressively increases towards the bottom of the concrete slab. This means that the reinforcing bars and the inner temperature of the slab was higher than +9.7 °C, and it reached +23 °C at the bottom of the slab once the influence of environmental conditions were considered. It should be noted that, in Figure 7, the variation of the ambient temperature did not change the temperature on top of the slab because such concrete surface is directly under the ethane tank and not exposed to the air.

Figure 8 compares the FE results against the measured temperature of the two Datasets (32 locations shown in Appendix A). It is shown that the results from the FE model match well the field data within a good degree of accuracy (SD < 5%). It should be noted that the

first set of temperature measurements (Dataset 1) at the bottom of the slab was obtained just after the leakage of ethane was observed, whereas the Dataset 2 was collected a week after the repair work was completed in the welded joints.

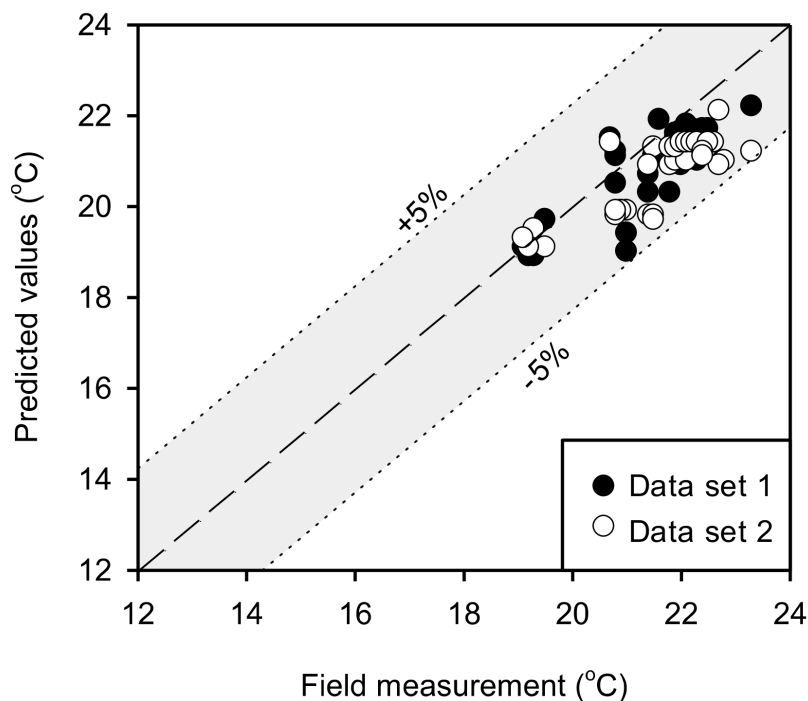


Figure 8. Comparison between FE simulation and measured temperature at the bottom of concrete slab.

The results from this case study show that numerical simulations can effectively assist in assessing the structural integrity of concrete foundations subjected to low temperature, provided there is sufficient and good quality field data. The FE results show that the ambient temperature at the site must be taken into account in the thermal analysis of foundations as that presented in this study. Simulations of two measured datasets show quite similar temperature distributions within a $\pm 5\%$ variation range. This indicates that the simplified heat transfer equation for porous media (Equation (2)) was sufficiently accurate to model the ethane leakage in the concrete foundation. Moreover, the results also confirm that reinforcing bars can be neglected in the thermal analysis of massive concrete slabs. Likewise, it should be noted that a simple FE modeling approach (that ignored the moisture in the concrete pores) was adopted in this study because the inspections did not reveal defects or spalls in the concrete slab. However, more complex FE modeling may be necessary to examine the moisture transport in concrete in other cases such as concrete exposed to fire (where high gas pressure can induce spalling of the concrete i.e., [45,46]), or when concrete is exposed to extremely low temperatures (below $-20\text{ }^{\circ}\text{C}$). This type of analysis could be used to assess the potential service of the structures subjected to continuous temperature gradients. In this case, however, the analysis should include the reinforcing bars as corrosion could also occur (and even before concrete deterioration due to excessive pore pressure). Based on the evidence from visual inspections, field measurements, NDTs and results from the numerical analyses, it can be concluded that the ethane leakage was unlikely to affect the mechanical properties of the concrete and reinforcing bars in the foundation. Annual inspections are being carried out to monitor the condition of the structure. At the present time (April 2022), the foundation has no signs of structural deterioration.

6. Conclusions

This article presents a case study on the thermal assessment of an RC foundation exposed to low temperatures. The foundation supports a large tank of a petrochemical plant and stores low-temperature ethane ($-89\text{ }^{\circ}\text{C}$). The ethane leaked to the RC foundation shortly after the tank started operations, which in turn produced condensation in the concrete slab of the foundation and raised structural safety concerns. An FE model of the concrete foundation was developed, and this proved to be an effective tool that provided further insight into the thermal behaviour of the slab. Based on the field inspections and numerical analysis presented in this study, the following conclusions can be drawn:

- The FE results show that the ambient temperature at the site must be taken into account in the thermal analysis of foundations, as presented in this study. When the ambient temperature recorded during the field temperature measurements was considered in the analysis, the temperatures calculated by the FE model agreed well with the measured values. The average of the ratios of measured temperatures to FE results was $\text{Exp}/\text{FE} = 1.03$, with a standard deviation $\text{SD} = 0.03$ for Dataset 1. The corresponding values were $\text{Exp}/\text{FE} = 1.05$ and $\text{SD} = 0.04$ for Dataset 2.
- The FE results also showed that the temperature progressively increases towards the bottom of the concrete slab. This means that the reinforcing bars and the inner temperature of the slab was higher than $+9.7\text{ }^{\circ}\text{C}$, and it reached $+23\text{ }^{\circ}\text{C}$ at the bottom of the slab once the influence of environmental conditions were considered. This indicates that the simplified heat transfer equation for porous media (Equation (2)) was sufficiently accurate to model the ethane leakage in the concrete foundation. Moreover, the results also confirm that reinforcing bars can be neglected in the thermal analysis of massive concrete slabs.
- Based on the evidence from visual inspections, field measurements, nondestructive testing and results from the FE analyses, it can be concluded that the ethane leakage was unlikely to affect the mechanical properties of the concrete and reinforcing bars in the foundation. Annual inspections are being carried out to monitor the condition of the structure. The approaches, methods and techniques presented in this article proved suitable to solve the practical and scientific challenges involved in the structural assessment and repairs of this large special structure. Accordingly, they can serve as useful reference and guidance for engineers and practitioners working in the field of forensic engineering.

Author Contributions: Conceptualization, T.I. and C.W.; methodology, T.I.; software, C.W.; validation, T.I. and P.A.; formal analysis, T.I.; investigation, P.A.; writing—original draft preparation, T.I.; writing—review and editing, C.W. and F.P.F.; visualization, C.H.; supervision, R.G. All authors have read and agreed to the published version of the manuscript.

Funding: This research was funded by a Walailak University research grant (contract no. WU 64252).

Institutional Review Board Statement: Not applicable.

Data Availability Statement: Not applicable.

Acknowledgments: This research was financially supported by the new strategic research project (P2P), Walailak University, Thailand. The authors are also thankful to International Engineering Consultants Co., Ltd., (IEC-Thailand) and PTT Global Chemical Public Company Limited, for providing access to the results from the field temperature measurements.

Conflicts of Interest: The authors declare no conflict of interest.

Appendix A

Table A1. Predicted temperature at bottom of concrete slab and field measurements.

| Locations ID | Field Measured Data Exp. (°C) | | Numerical FE Predictions (°C) for Dataset 1 | | Numerical Predictions (°C) for Dataset 2 | |
|--------------|-------------------------------|----------------------|---|----------------|--|----------------|
| | Dataset 1 | Dataset 2 | $T_a = n/a$ | T_a Included | $T_a = n/a$ | T_a Included |
| 1 | 21.0 | 19.5 | 13.7 | 19.0 | 13.7 | 19.1 |
| 2 | 21.0 | 19.3 | 14.0 | 19.4 | 14.0 | 19.5 |
| 3 | 20.9 | 19.2 | 14.3 | 19.9 | 13.7 | 19.1 |
| 4 | 20.8 | 19.1 | 14.8 | 20.5 | 13.8 | 19.3 |
| 5 | 21.4 | 23.0 | 14.9 | 20.7 | 15.3 | 21.4 |
| 6 | 21.4 | 21.5 | 14.6 | 20.3 | 15.3 | 21.3 |
| 7 | 21.8 | 21.4 | 14.7 | 20.3 | 14.2 | 19.8 |
| 8 | 23.3 | 21.5 | 16.0 | 22.2 | 14.2 | 19.8 |
| 9 | 19.3 | 21.5 | 13.6 | 18.9 | 14.1 | 19.7 |
| 10 | 19.2 | 21.0 | 13.6 | 18.9 | 14.2 | 19.9 |
| 11 | 19.2 | 20.9 | 13.7 | 19.0 | 14.2 | 19.9 |
| 12 | 19.1 | 20.8 | 13.8 | 19.1 | 14.2 | 19.8 |
| 13 | 19.5 | 20.8 | 14.2 | 19.7 | 14.2 | 19.9 |
| 14 | 20.7 | 23.3 | 15.5 | 21.5 | 15.2 | 21.2 |
| 15 | 20.8 | 22.7 | 15.2 | 21.1 | 15.8 | 22.1 |
| 16 | 20.8 | 22.8 | 15.3 | 21.2 | 15.0 | 21.0 |
| 17 | 21.5 | 22.7 | 15.2 | 21.1 | 14.9 | 20.9 |
| 18 | 21.6 | 21.8 | 15.8 | 21.9 | 15.0 | 20.9 |
| 19 | 22.0 | 23.0 | 15.1 | 20.9 | 15.0 | 21.0 |
| 20 | 23.0 | 22.1 | 15.2 | 21.1 | 15.0 | 21.0 |
| 21 | 22.3 | 21.8 | 15.2 | 21.0 | 15.2 | 21.3 |
| 22 | 22.9 | 21.9 | 15.6 | 21.7 | 15.3 | 21.3 |
| 23 | 22.5 | 22.0 | 15.7 | 21.7 | 15.3 | 21.4 |
| 24 | 22.2 | 22.1 | 15.6 | 21.7 | 15.3 | 21.4 |
| 25 | 22.2 | 22.2 | 15.7 | 21.7 | 15.3 | 21.4 |
| 26 | 22.1 | 22.3 | 15.5 | 21.4 | 15.3 | 21.4 |
| 27 | 21.9 | 22.5 | 15.3 | 21.3 | 15.2 | 21.3 |
| 28 | 23.0 | 23.0 | 15.5 | 21.5 | 15.3 | 21.4 |
| 29 | 21.9 | 22.5 | 15.6 | 21.6 | 15.3 | 21.4 |
| 30 | 22.0 | 22.4 | 15.6 | 21.6 | 15.2 | 21.2 |
| 31 | 22.1 | 22.4 | 15.7 | 21.8 | 15.1 | 21.1 |
| 32 | 22.0 | 21.4 | 15.3 | 21.3 | 14.9 | 20.9 |
| | | <i>Mean (Exp/FE)</i> | <i>1.43</i> | <i>1.03</i> | <i>1.47</i> | <i>1.05</i> |
| | | <i>SD (Exp/FE)</i> | <i>0.05</i> | <i>0.03</i> | <i>0.04</i> | <i>0.04</i> |

Note: Field data from Dataset 1 was measured by the stakeholder. Dataset 2 was measured by the authors as shown in Figure A1.

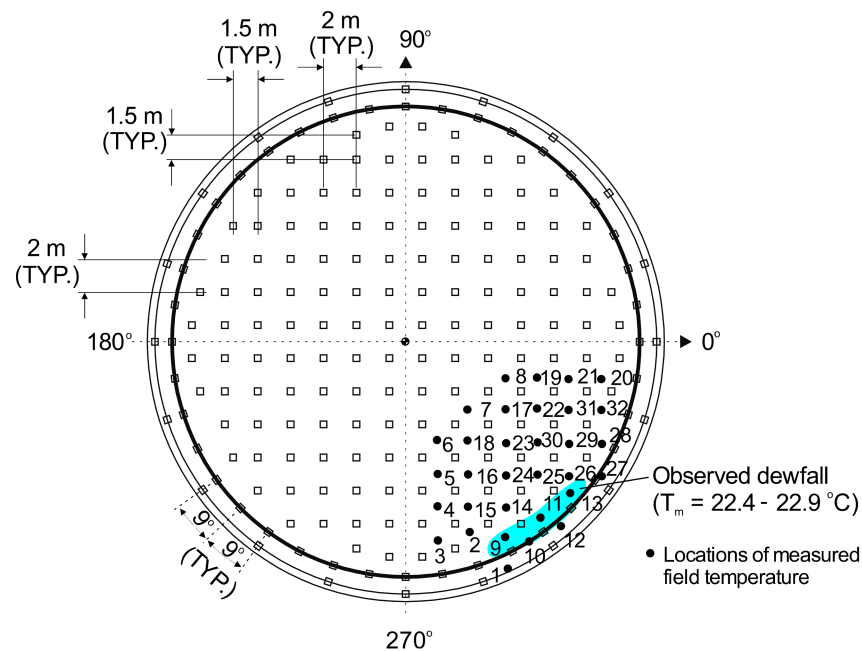


Figure A1. Locations of field temperature measurements and typical pile spacing (in meters).

References

1. Le May, I. Structural integrity and petrochemical industry. *Energy Mater.* **2008**, *3*, 208–219. [[CrossRef](#)]
2. Mieno, F. The Eastern Seaboard Development Plan and Industrial Cluster in Thailand: A Quantitative Overview. In *Aid as Handmaidens for the Development of Institutions: A New Comparative Perspective*; Nissanke, M., Shimomura, Y., Eds.; Palgrave Macmillan: London, UK, 2013; pp. 81–105.
3. Azadeh, A.; Salehi, V.; Arvan, M.; Dolatkah, M. Assessment of resilience engineering factors in high-risk environments by fuzzy cognitive maps: A petrochemical plant. *Saf. Sci.* **2014**, *68*, 99–107. [[CrossRef](#)]
4. Moradi, B. Risk-Based Inspection Technique and the Benefits of Its Implementation in Improving the Process Management System of Oil, Gas and Petrochemical Industries: A Review Study. *J. Saf. Promot. Inj. Prev.* **2020**, *8*, 158–171. [[CrossRef](#)]
5. Si, H.; Ji, H.; Zeng, X. Quantitative risk assessment model of hazardous chemicals leakage and application. *Saf. Sci.* **2012**, *50*, 1452–1461. [[CrossRef](#)]
6. Ghani, U.; Shabbir, F.; Khan, K. Effect of temperature on different properties of concrete. In Proceedings of the 31st Conference Our World in Concrete and Structures, Singapore, 16–17 August 2006.
7. Lee, G.C.; Shih, T.S.; Chang, K.C. Mechanical Properties of Concrete at Low Temperature. *J. Cold Reg. Eng.* **1988**, *2*, 13–24. [[CrossRef](#)]
8. Collins, A.R. The Destruction of Concrete by Frost. *J. Inst. Civ. Eng.* **1944**, *23*, 29–41. [[CrossRef](#)]
9. Rostásy, F.S.; Schneider, U.; Wiedemann, G. Behaviour of mortar and concrete at extremely low temperatures. *Cem. Concr. Res.* **1979**, *9*, 365–376. [[CrossRef](#)]
10. Filiatrault, A.; Holleran, M. Stress-strain behavior of reinforcing steel and concrete under seismic strain rates and low temperatures. *Mater. Struct.* **2001**, *34*, 235–239. [[CrossRef](#)]
11. Liu, S.; Gu, X.L.; Huang, Q.H.; Zhang, W.P. Experimental Study on the Bending Behavior of Reinforced Concrete Beams under Super-Low Temperature. In *Earth and Space 2021: Engineering, Science, Construction, and Operations in Challenging Environments*; ASCE: Reston, VA, USA, 2021; pp. 3537–3544.
12. DeRosa, D.; Hoult, N.A.; Green, M.F. Effects of varying temperature on the performance of reinforced concrete. *Mater. Struct.* **2015**, *48*, 1109–1123. [[CrossRef](#)]
13. Montejo, L.; Asce, S.; Sloan, J.; Asce, A.; Kowalsky, M.; Kowalsky, J.; Hassan, T. Cyclic Response of Reinforced Concrete Members at Low Temperatures. *J. Cold Reg. Eng.* **2008**, *22*, 79–102. [[CrossRef](#)]
14. Sargam, Y.; Faytarouni, M.; Riding, K.; Wang, K.; Jahren, C.; Shen, J. Predicting thermal performance of a mass concrete foundation—A field monitoring case study. *Case Stud. Constr. Mater.* **2019**, *11*, e00289. [[CrossRef](#)]
15. Yan, J.-B.; Xie, J. Behaviours of reinforced concrete beams under low temperatures. *Constr. Build. Mater.* **2017**, *141*, 410–425. [[CrossRef](#)]
16. Monfore, G.E.; Lentz, A.E. *Physical Properties of Concrete at Very Low Temperatures*; Portland Cement Association, Research and Development Laboratories: Washington, DC, USA, 1962.
17. Li, W.; Sun, W.; Jiang, J. Damage of concrete subjected to simultaneous fatigue load and thermal effect. *Mag. Concr. Res.* **2012**, *64*, 35–42. [[CrossRef](#)]

18. API 653; Tank Inspection, Repair, Alteration, and Reconstruction. The American Petroleum Institute: Washington DC, USA, 2014.
19. BS EN 14620-3:2006; Design and Manufacture of Site Built, Vertical, Cylindrical, Flat-Bottomed Steel Tanks for the Storage of Refrigerated, Liquefied Gases with Operating Temperatures between 0 °C and –165 °C—Part 3: Concrete Components. British Standards Institution: London, UK, 2006.
20. Kong, L.-P.; Qiao, L.; Xiao, Y.-Y.; Li, Q.-W. A study on heat transfer characteristics and pile group influence of enhanced heat transfer energy piles. *J. Build. Eng.* **2019**, *24*, 100768. [[CrossRef](#)]
21. Sharifi, N.P.; Freeman, G.E.; Sakulich, A.R. Using COMSOL modeling to investigate the efficiency of PCMs at modifying temperature changes in cementitious materials—Case study. *Constr. Build. Mater.* **2015**, *101*, 965–974. [[CrossRef](#)]
22. Yang, W.; Zhang, L.; Zhang, H.; Wang, F.; Li, X. Numerical investigations of the effects of different factors on the displacement of energy pile under the thermo-mechanical loads. *Case Stud. Therm. Eng.* **2020**, *21*, 100711. [[CrossRef](#)]
23. Cawley, P. Non-destructive testing—Current capabilities and future directions. *Proc. Inst. Mech. Eng. Part L J. Mater. Des. Appl.* **2001**, *215*, 213–223. [[CrossRef](#)]
24. Dwivedi, S.K.; Vishwakarma, M.; Soni, P.A. Advances and Researches on Non Destructive Testing: A Review. *Mater. Today Proc.* **2018**, *5*, 3690–3698. [[CrossRef](#)]
25. Sinclair, T.; Malkin, R. Sensors for Ultrasonic Nondestructive Testing (NDT) in Harsh Environments. *Sensors* **2020**, *20*, 456. [[CrossRef](#)]
26. Weber, B.; Dauti, D.; Dal Pont, S. COMSOL Implementation of a porous media model for simulating pressure development in heated concrete. In Proceedings of the COMSOL Conference 2016, Munich, Germany, 12–14 October 2016; p. 6.
27. Žmindač, M.; Novák, P.; Dekýš, V.; Pelagić, Z. Finite Element Thermo-mechanical Transient Analysis of Concrete Structure. *Procedia Eng.* **2013**, *65*, 224–229. [[CrossRef](#)]
28. Huang, H.; Garcia, R.; Guadagnini, M.; Pilakoutas, K. Effect of section geometry on development of shrinkage-induced deformations in box girder bridges. *Mater. Struct.* **2017**, *50*, 222. [[CrossRef](#)]
29. Jana, D. Cracking of residential concrete foundations in eastern Connecticut, USA from oxidation of pyrrhotite. *Case Stud. Constr. Mater.* **2022**, *16*, e00909. [[CrossRef](#)]
30. Toyo Engineering Corporation. *The Thermal (Low Temperature) Effect to T-4801 Ethane Tank Foundation Due to the Leakage of Ethane*; Technical Report R0 20110207; Toyo Engineering Corporation: Bangkok, Thailand, 2011.
31. ASTM A240; Standard Specification for Chromium and Chromium-Nickel Stainless Steel Plate, Sheet, and Strip for Pressure Vessels and for General Applications. ASTM International: West Conshohocken, PA, USA, 2020. [[CrossRef](#)]
32. ASTM E1002-11; Standard Practice for Leaks Using Ultrasonics. ASTM International: West Conshohocken, PA, USA, 2018. [[CrossRef](#)]
33. Imjai, T.; Tungsanga, K. Finite Element Analysis on Temperature Distribution of Ethane Storage Tank Concrete Foundation—A Case Study. In Proceedings of the International Conference on Advances in Computational Mechanics (ACOME), Ho Chi Minh City, Vietnam, 14–16 August 2012.
34. International Engineering Consultants Co.Ltd. *Engineering Verification of T-4801 Ethane Tank Foundation Strength*; Technical Report No. IEC-T4801-01; International Engineering Consultants Co., Ltd.: Bangkok, Thailand, 2011; p. 32.
35. ACI 364. 1; Guide for Evaluation of Concrete Structures Prior to Rehabilitation. American Concrete Institute: Farmington Hills, MI, USA, 1999.
36. API 12C; Specification for Welded Oil Storage Tanks. The American Petroleum Institute: Washington, DC, USA, 1962.
37. ACI 318-14; Building Code Requirements for Structural Concrete. American Concrete Institute: Farmington Hills, MI, USA, 2014.
38. ASTM C177-19; Standard Test Method for Steady-State Heat Flux Measurements and Thermal Transmission Properties by Means of the Guarded-Hot-Plate Apparatus. ASTM International: West Conshohocken, PA, USA, 2019. [[CrossRef](#)]
39. Bernuzzi, C.; Cordova, B. *Structural Steel Design to Eurocode 3 and AISC Specifications: Bernuzzi/Structural Steel Design to Eurocode 3 and AISC Specifications*; John Wiley & Sons: Hoboken, NJ, USA, 2016.
40. Comsol Multiphysics. *Comsol v. 5.4 Heat Transfer Module User's Guide*; Comsol Multiphysics: Burlington, MA, USA, 2008.
41. Nield, D.A. Effects of local thermal nonequilibrium in steady convective processes in a saturated porous medium: Forced convection in a channel. *J. Porous Media* **1998**, *1*, 181–186.
42. Nield, D.A.; Bejan, A. *Convection in Porous Media*, 4th ed.; Springer: New York, NY, USA, 2013.
43. Gasch, T.; Ericsson, D. Thermally-induced cracking of a concrete arch dam using COMSOL Multiphysics. In Proceedings of the 14th ICOLD International Benchmark Workshop on Numerical Analysis of Dams, Stockholm, Sweden, 6–8 September 2017.
44. Johnson, K.R. *Thermal Integrity Analysis of Concrete Bridge Foundations Using COMSOL Multiphysics® Software*; Comsol Multiphysics: Burlington, MA, USA, 2017.
45. da Amorim Coelho, N.; Pedroso, L.J.; da Silva Rêgo, J.H.; Nepomuceno, A.A. Use of ANSYS for thermal analysis in mass concrete. *J. Civ. Eng. Archit.* **2014**, *8*, 860–868. [[CrossRef](#)]
46. Isgor, O.B.; Razaqpur, A.G. Finite element modeling of coupled heat transfer, moisture transport and carbonation processes in concrete structures. *Cem. Concr. Compos.* **2004**, *26*, 57–73. [[CrossRef](#)]